Disjunctive Normal Parametric Level Set With Application to Image Segmentation

Fitsum Mesadi, *Student Member, IEEE*, Mujdat Cetin, *Member, IEEE*, and Tolga Tasdizen, *Senior Member, IEEE*

***Abstract*— Level set methods are widely used for image segmentation because of their convenient shape representation for numerical computations and capability to handle topological changes. However, in spite of the numerous works in the literature, the use of level set methods in image segmentation still has several drawbacks. These shortcomings include formation of irregularities of the signed distance function, sensitivity to initialization, lack of locality, and expensive computational cost, which increases dramatically as the number of objects to be simultaneously segmented grows. In this paper, we propose a novel parametric level set method called disjunctive normal level set (DNLS), and apply it to both two-phase (single object) and multiphase (multiobject) image segmentations. DNLS is a differentiable model formed by the union of polytopes, which themselves are created by intersections of half-spaces. We formulate the segmentation algorithm in a Bayesian framework and use a variational approach to minimize the energy with respect to the parameters of the model. The proposed DNLS can be considered as an open framework that allows the use of different appearance models and shape priors. Compared with the conventional level sets available in the literature, the proposed DNLS has the following major advantages: it requires significantly less computational time and memory, it naturally keeps the level set function regular during the evolution, it is more suitable for multiphase and local region-based image segmentations, and it is less sensitive to noise and initialization. The experimental results show the potential of the proposed method.**

***Index Terms*— Level set, disjunctive normal forms, segmentation, parametric level set, multiphase level set, variational, Bayesian methods.**

I. Introduction

THE level set method, first introduced by Osher and Sethian [1], is a popular technique for the evolution of interfaces. The technique has a wide range of applications in image processing, computer graphics, computational geometry, optimization, and computational fluid dynamics. The basic idea behind the level set method is to represent contours as the zero level set of an implicit function defined in a higher dimension, usually referred to as the level set function, and formulate the evolution of the contour through the evolution of the level set function [2].

Manuscript received July 27, 2016; revised December 27, 2016; accepted February 25, 2017. Date of publication March 15, 2017; date of current version April 11, 2017. This work was supported in part by NSF under Grant IIS-1149299, in part by NIH under Grant 1R01-GM098151-01, in part by TUBITAK under Grant 113E603, and in part by TUBITAK under Grant 2221. The associate editor coordinating the review of this manuscript and approving it for publication was Dr. Yonggang Shi.

F. Mesadi and T. Tasdizen are with the Department of Electrical and Computer Engineering, The University of Utah, Salt Lake City, UT 84112 USA (e-mail: fitsum.mesadi@yahoo.com).

M. Cetin is with the Faculty of Engineering and Natural Sciences, Sabanci University, 34956 Istanbul, Turkey.

Color versions of one or more of the figures in this paper are available online at http://ieeexplore.ieee.org.

Digital Object Identifier 10.1109/TIP.2017.2682980

A. Related Work

The ability of the level set method to handle topological changes automatically, and its convenient representation of regions and their boundaries on the pixel grid without the need of complex data structures, has made the level set suitable for image segmentation applications [3], [4].

The Bayesian formulation of Geman and Geman [5] and the energy functional of Mumford and Shah (MS) [6] had a significant impact on the understanding of image segmentation by transforming the handling of the problem from a heuristic approach to algorithms with sound mathematical concepts [7]. Brox and Cremers [7] have shown the equivalence of the MS energy functional and the Bayesian model. Given an image $I : \Omega \rightarrow \mathbb{R}$ with $\Omega_{1,\ldots,R}$ regions, the general energy functional that unifies the MS and the Bayesian method for image segmentation [4], [8] is given as

$$E(\Omega_r, P_r) = \sum_{r=1}^{R} \int_{\Omega_r} -\log \mathcal{P}_r \mathbf{dx} + \upsilon |S| \tag{1}$$

where $\mathcal{P}_r$ models the probability density functions (pdf) of region Ω_r, $|S|$ represents the total length of the boundary of the disjoint regions, and υ is a constant weighting parameter. The first term in (1) maximizes the *a posterior* probability of pixels being assigned to the correct region, and the second term minimizes the boundary length. Minimizing equation (1) is difficult since the first term is acting on the two-dimensional (2D) image domain while the second term is a one-dimensional (1D) curve. The use of a level set framework helps to elegantly handle this problem, since the contour S is embedded into the image domain and represented by the zero level set of the level set function Φ. For instance, the level set formulation of (1) for a two-phase (two regions) segmentation can be written as

$$E = -\int_{\Omega} H(\Phi) \log \mathcal{P}_1 + (1 - H(\Phi)) \log \mathcal{P}_2 + \upsilon |\nabla H(\Phi)| \mathbf{dx} \tag{2}$$

where the level set function $\Phi > 0$ for region Ω_1 and $\Phi < 0$ for region Ω_2. The Heaviside function $H(\Phi) = 0$ for $\Phi < 0$ and $H(\Phi) = 1$ for $\Phi > 0$.

Although the use of a level set framework in image segmentation has significant advantages, the conventional level set formulation has several major drawbacks: expensive computational cost, formation of irregularities of the signed distance

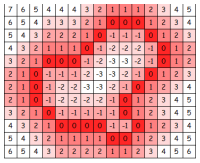

Fig. 1. SDF, Φ.

function, sensitivity to noise and initialization, and lack of locality. Next, we elaborate these shortcomings, give the prominent works in the literature that address them, and then discuss the remaining challenges that we attempt to solve in this paper.

1) Computational Cost: Level set implementation is computationally expensive, since it increases the dimension of the problem by one. Modifications such as fast marching [9] and sparse methods [10] have been proposed to improve the computational time of level set evolution. However, level set evolution is still relatively slow [11]. This is mainly because the gradient descent methods used in level set evolution need a large number of iterations, since their time step is limited by the standard Courant-Friedrichs-Lewy (CFL) condition [12], [13] (CFL is also essential for the numerical stability of the iterative scheme [12], [13]).

2) Level Set Function Irregularity: The level set function, Φ, develops irregularities, such as a very sharp or flat shape, during evolution [2]. Figure 1 shows an example of a regular signed distance function (SDF), Φ, which is usually used as a level set function. Irregularities in the function cause numerical errors and eventually destroy the stability of the level set evolution. In order to overcome these irregularities, some of the techniques employed are periodically re-initializing of the level set function, and adding a regularizing term that forces the level set function to be close to a signed distance function [14], [15]. However, the re-initialization method has the undesirable effects of moving the level set from its original location, expensive computational cost, and blocking the emerging of new contours; whereas, the regularizing terms also add computational cost and still cannot guarantee the smoothness of the signed distance functions [14], [15].

3) Sensitivity to Noise: Segmentation of noise corrupted images using conventional level set methods is challenging. The recently proposed level set segmentation methods in [14] and [15] have more capability to handle significant noise level corruption. However, these latest techniques still require tuning of parameters. For instance, by using larger weight for the boundary length term (see equation 1) which forces the boundary to be shorter, these methods can make the segmentation less sensitive to noise. However, forcing the boundary to be shorter has the unintended consequence of making the contour stiff resulting in reduced flexibility to handle complex shapes.

4) Multiphase Segmentation Challenges: For segmentation of an image into more than two regions, several algorithms have been proposed in the literature using the level set method [4], [16]–[19]. To segment multiphase images, one level set function Φ_r can be used for each region Ω_r in equation (1). However, this simple method can result in overlap of the different regions and creation of gaps. To overcome these challenges, extra coupling forces are introduced in [16] and [18]. Although modeling each object independently with its own level set function has some advantages, the computational cost and memory requirements become daunting as the number of objects to be segmented grows [19]. Vese and Chan [20] proposed a multiphase level set framework that requires $\log_2 R$ level set functions to segment R regions. Although the method in [20] is relatively computationally attractive, it is more convenient to have a unique level set for each object in applications such as tracking of the individual objects and use of their shape priors. The computational cost of all the above multiphase level set methods increases significantly as the number of objects to be simultaneously segmented grows. In general, in addition to their expensive computational cost and memory requirements, most multiphase level set methods in the literature are also very sensitive to initialization [4], [20].

5) Lack of Locality: The current level set methods available in the literature lack a locality property. That is, signed distance functions do not give unique local information. For instance, from the signed distance function shown in Fig. 1, we can see that all the points that are at the same distance from the zero level set are given the same value, even though the points are far from each other; hence, there is no way to uniquely identity a given local region. This prohibits the use of powerful local appearance models in level set methods [21]. For instance, a pedestrian wearing multicolored clothes requires modeling of her appearance at a small local scale, instead of a single global appearance model normally obtained by using a conventional level set to represent the person.

Lankton and Tannenbaum [22] proposed a mathematical framework for localizing region-based energies in the level set segmentation method. Localizing of the region-based energy is necessary when the image features are not spatially invariant, for instance due to the bias field in MR images. Recently, several local region-based segmentation methods have appeared in the literature for inhomogeneous image segmentation [7], [23]–[25]. What all the inhomogeneous image segmentation methods in the literature have in common is that they compute local region statistics by convolution of the image with a truncated Gaussian kernel or a box of fixed size around each pixel. This convolution significantly increases the computational time.

In order to limit the computational cost and also minimize irregularities of the level set function, parametric level set methods have been proposed in the literature [3], [12], [26]–[31]. The minimization of the functional is directly obtained in terms of the radial basis function or B-spline coefficients. These parametric level set formulations require less computational cost due to the low-order representation and the possibility of using larger step sizes. Although these parametric level set methods simplify the challenges involved in keeping the regularities of the level set function, they still require re-normalization of the level set function during the evolution process [3]. In addition, when applied to multiphase and local region-based image segmentations, the parametric

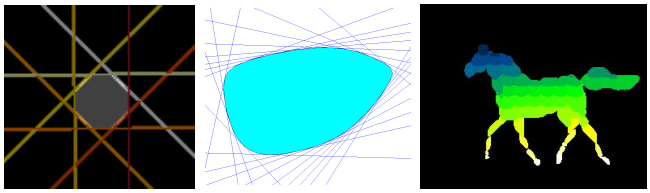

a b c

Fig. 2. Illustration of the DNLS shape representation. In (a), the intersection of 8 discriminant half-spaces is used to create a polytope. In (b), a larger number of half-spaces is used to create a smoother polytope. In (c), the union of many polytopes are used to represent a horse shape (each polytope is shown with a different intensity/color level).

level set currently available in the literature has the same drawbacks as the conventional nonparametric level set method.

B. Contributions

In this paper, we propose a novel parametric level set method called Disjunctive Normal Level Set (DNLS), and apply it to both two-phase and multiphase image segmentations. The DNLS is based on an implicit and parametric shape model called Disjunctive Normal Shape Models (DNSM). The DNSM has recently been used for a single object segmentation: to model the shape and appearance priors of objects in [32]–[34], and as an interactive segmentation framework in [35]. The DNLS approximates the characteristic function of a shape as a union of convex polytopes which themselves are represented as intersections of half-spaces. Figure 2(a) shows how the conjunctions of eight half-spaces form a convex polytope. If we use more half-spaces, we can represent smoother convex polytopes as shown in Fig. 2(b). Our DNLS uses the disjunction of many convex polytopes to represent complex shapes, as shown in Fig. 2(c).

DNLS is a differentiable level set shape representation that allows the use of variational approaches. The major contributions of this paper include a novel parametric level set representation and Bayesian framework for two-phase and multiphase image segmentations using the proposed level set. Compared to the conventional level set formulations, the proposed DNLS has the following major advantages:

- *Lower computational cost*: Two major factors contribute to the reduction in computational time for the proposed DNLS method. First, parametric representation of the DNLS level set results in a lower-dimensional problem. Second, the time step of our DNLS is not limited by the standard CFL condition; hence, we can use a larger step size during the initial stages of the evolution, resulting in fewer number of iterations.
- *Regular level set function*: The DNLS is not based on a signed distance function, and the level set function remains naturally regular during the evolution. Hence, re-initialization (and all the drawbacks that comes with it) is completely avoided.
- *Insensitivity to Noise*: The proposed DNLS is less sensitive to noise, and does not need tuning of any length term.
- *Efficient and robust multiphase level set framework*: The DNLS we propose in this paper has the highly desirable properties that it is less sensitive to initialization, and its computational cost and memory requirement remains almost constant as the number of objects to be segmented grows, while also having the capability to represent each object with a unique level set. These properties are mainly because the DNLS is formed by union of many polytopes, each of which can be treated as a level set function and assigned to different objects (or phases).
- *Locality information*: The DNLS we propose has strong locality due to its discriminants and polytopes that form the model, which can be seen from the differently colored local regions in Fig. 2(c). The locality property of the DNLS allows the use of powerful local appearance models, and can also reduce the computational cost of local region-based multiphase segmentations.

The rest of the paper is organized as follows. In section II, we present the DNLS shape representation. Section III introduces how the DNLS can be used in image segmentation. In section IV, we present an application of the proposed level set for two-phase image segmentation. In section V, we describe our multiphase level set framework and show how it is used for simultaneous segmentation of multiple regions. In section VI, we provide qualitative and quantitative analysis of the proposed DNLS segmentation framework and compare it with the latest level set image segmentation methods in the literature by using different phantom, natural, and medical images. Finally, section VII provides the conclusion. Preliminary results of this work have been presented at the ICIP 2016 conference [36]. Compared to [36] this journal version: provides detailed explanations and derivations of the algorithms, formulates the proposed algorithm in a Bayesian framework, gives a generic approach that can be used with any appearance feature, shows the capability of the proposed DNLS method for both homogenous and inhomogeneous image segmentations, and provides a significantly expanded experimental section.

II. Disjuctive Normal Level Set

Consider the characteristic function $f : \mathbf{R}^D \rightarrow \mathbf{B}$ where $\mathbf{B} = \{0, 1\}$. Let $\Omega^+ = \{\mathbf{x} \in \mathbf{R}^D : f(\mathbf{x}) = 1\}$. Let us approximate Ω^+ as the union of N convex polytopes $\tilde{\Omega}^+ = \cup_{i=1}^{N} \mathcal{P}_i$, where the i'th polytope is defined as the intersection of $\mathcal{P}_i = \cap_{j=1}^{M} \mathcal{H}_{ij}$ of M half-spaces. H_{ij} is defined in terms of its indicator function

$$h_{ij}(\mathbf{x}) = \begin{cases} 1, & \sum_{k=0}^{D} w_{ijk} x_k + b_{ij} \geq 0 \\ 0, & otherwise, \end{cases} \tag{3}$$

where w_{ijk} and b_{ij} are the weights and the bias term, and D is the dimension. Since any Boolean function can be written in disjunctive normal form [37], we can construct

$$\tilde{f}(\mathbf{x}) = \bigvee_{i=1}^{N} \underbrace{\left(\bigwedge_{j=1}^{M} h_{ij}(\mathbf{x}) \right)}_{B_i(\mathbf{x})}, \tag{4}$$

such that $\tilde{\Omega}^+ = \{\mathbf{x} \in \mathbf{R}^n : \tilde{f}(\mathbf{x}) = 1\}$. Since $\tilde{\Omega}^+$ is an approximation to Ω^+, it follows that $\tilde{f}$ is an approximation

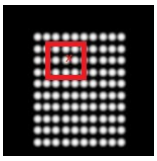

Fig. 3. Regularly distributed polytopes.

to f. Our next step is to provide a differentiable approximation to $\tilde{f}$, which is important because it allows us to use variational approaches; in other words, it allows us to formulate various energy functions and to minimize them with respect to the parameters of the model. First, the conjunction of binary variables $\bigwedge_{j=1}^{M} h_{ij}(\mathbf{x})$ can be replaced by the product $\prod_{j=1}^{M} h_{ij}(\mathbf{x})$. Then, using De Morgan's laws [37] we replace the disjunction of the binary variables $\bigvee_{i=1}^{N} B_i(\mathbf{x})$ with $\neg \bigwedge_{i=1}^{N} \neg B_i(\mathbf{x})$, which in turn can be replaced by the expression $1-\prod_{i=1}^{N}(1-B_i(\mathbf{x}))$. Finally, we approximate $h_{ij}(\mathbf{x})$ with logistic sigmoid functions $\sigma_{ij}(\mathbf{x}) = \frac{1}{1+e^{\sum_{k=0}^{D} w_{ijk}x_k+b_{ij}}}$ to get the differentiable approximation of the characteristic function $\hat{f}(\mathbf{x})$

$$\hat{f}(\mathbf{x};\mathbf{W}) = 1 - \prod_{\substack{i=1 \\ i\in\aleph(\mathbf{x})}}^{N} \left(1 - \underbrace{\prod_{j=1}^{M} \frac{1}{1+e^{\sum_{k=0}^{D} w_{ijk}x_k+b_{ij}}}}_{g_i(\mathbf{x})} \right), \quad (5)$$

where $\mathbf{x} = \{x, y, 1\}$ for two-dimensional (2D) shapes and $\mathbf{x} = \{x, y, z, 1\}$ for three-dimensional (3D) shapes. By appending 1 to the pixel coordinates $\mathbf{x}$, we use w_{ijk} to represent both the weights and the biases in the rest of the paper. $\mathbf{W} = \{w_{ijk}\}$ are the discriminant parameters, and $\aleph(\mathbf{x})$ is the list of polytopes that are in the neighborhood of the location $\mathbf{x}$. $g_i(\mathbf{x})$ represents the i^{th} polytope.

The only adaptive parameters in equation (5) are the weights (w_{ijk}) and biases (b_{ij}) of the first layer of logistic sigmoid functions $\sigma_{ij}(\mathbf{x})$ that define the orientations and positions of the linear discriminants that form the shape boundary. In equation (5), $f(\mathbf{x}) : \mathbf{R}^D \rightarrow [0, 1]$, and the level set $f(x) = 0.5$ represents the interface between the foreground $f(\mathbf{x}) > 0.5$ (inside the shape) and background $f(\mathbf{x}) < 0.5$ (outside the shape) regions. Therefore, the DNLS $f(x)$ is a continuous value between 0 and 1; hence, it is not a signed distance function and does not suffer from irregularities.

The DNLS formulation of equation (5) is similar to the DNSM shape model presented in [32] and [35], except for two modifications.

First, instead of using the application domain knowledge to decide on the small number of polytopes needed [32], [35], we use a large number of polytopes, N, in the DNLS formulation, and initialize the level set with regularly distributed polytopes (in the region of interest), as can be seen in Fig. 3. The use of dense initialization helps the DNLS to automatically capture complex shapes, detect small parts and holes, and provides a fast convergence speed. The initialization polytopes are approximated as discs (and spheres for 3D) of a fixed radius, using seed points that are regularly distributed in the region of interest. The initial disc approximation is obtained by choosing the parameters, w_{ijk}, as

$$w_{ijk} = \begin{cases} \cos\left(\frac{2\pi j}{M}\right), & k = 0 \\ \sin\left(\frac{2\pi j}{M}\right), & k = 1 \\ -\left(r + \left(C_x(i) \times \cos\left(\frac{2\pi(j-1)}{M}\right)\right)\right. & \\ \left. + \left(C_y(i) \times \sin\left(\frac{2\pi(j-1)}{M}\right)\right)\right), & k = 2 \end{cases} \quad (6)$$

where r is the radius of the initial disc. $C_x(i)$ and $C_y(i)$ are the center point coordinates for polytope i. In conventional level set methods, the initialization is carried out by generating a signed distance function using, for instance, a fast marching method. On the other hand, the initialization of our DNLS is generated efficiently using the closed-form equation given in (6).

Second, for computational efficiency, we use only the neighboring polytopes, $\aleph(\mathbf{x})$, for each location, $\mathbf{x}$, in the image. For instance, in Fig. 3 only the polytopes in the red box are used when evaluating the characteristic function, f, at location $\mathbf{x}$. Since the polytopes are regularly distributed in the image, each pixel has its own fixed set of polytopes, $\aleph(\mathbf{x})$, which can be precomputed. During the level set evaluation, the individual polytopes can grow, shrink, deform, disappear, and reappear.

III. Image Segmentation Using DNLS

The goal of DNLS-based image segmentation can be formulated as the estimation of the optimal DNLS parameters, $\mathbf{W} = \{w_{ijk}\}$, given an image $I : \Omega \rightarrow \mathbb{R}$. In the Bayesian framework, this can be computed by maximizing the posterior distribution

$$\mathcal{P}(\mathbf{W}/I) \propto \mathcal{P}(I/\mathbf{W})\mathcal{P}(\mathbf{W}) \quad (7)$$

The $\mathcal{P}(\mathbf{W})$ factor is the *a prior* probability of a certain partitioning $\mathbf{W}$. $\mathcal{P}(\mathbf{W})$ is a geometry-based factor for which a simple approach that minimizes the total boundary length (surface in 3D) or a sophisticated shape priors can be used [32].

The $\mathcal{P}(I/\mathbf{W})$ factor, in general, is approximated by an intensity distributions in the regions $r \in \{1, ..., R\}$, where the regions are formed by $\mathbf{W}$. Following a similar approach given in [7], and assuming independence of intensities at different locations $\mathbf{x}$, we can write $\mathcal{P}(I/\mathbf{W}) = \prod_{\mathbf{x}\in\Omega} \mathcal{P}(I(\mathbf{x})/\mathbf{W}, \mathbf{x})^{\mathbf{dx}}$, where $\mathbf{dx}$ is an infinitesimal bin size. With the partitioning of Ω by the DNLS parameters $\mathbf{W}$ into disjoint regions ($\Omega = \cup_r \Omega_r$, $\Omega_r \cap \Omega_j = \emptyset, \forall r \neq j$), $\mathcal{P}(I/\mathbf{W})$ over the whole image domain can be separated into products over the regions

$$\mathcal{P}(I/\mathbf{W}) = \prod_{r} \prod_{\mathbf{x}\in\Omega_r} P(I(\mathbf{x})/\mathbf{x} \in \Omega_r)^{\mathbf{dx}} \quad (8)$$

The most probable segmentation of a given image is then obtained by maximizing the posterior probability in equation (7), which is equivalent to minimizing its negative logarithm. Therefore, the energy to be minimized is given as

$$E(\mathbf{W}) = -\sum_{r=1}^{R} \int_{\Omega_r} \log \mathcal{P}_r(I(\mathbf{x}), \mathbf{x})\mathbf{dx} - \log \mathcal{P}(\mathbf{W}) \quad (9)$$

where $\mathcal{P}_r$ is the probability density of region r. Equation (9) is the DNLS-based equivalent of the general segmentation equation given in (1). Looking at equation (9), we can observe different image segmentation cases. When $R = 2$, we have a standard two-phase segmentation of an image into foreground and background regions. When $R > 2$, we have a multiphase segmentation case. We present these two cases in detail in sections IV and V, respectively. In addition, based on how $\mathcal{P}_r$ is modeled, we can have homogenous and inhomogeneous image segmentation cases. If the intensities in each region are assumed to be homogenous, $\mathcal{P}_r$ can be modeled as a Gaussian distribution with a constant mean, resulting in the popular piecewise constant case.

Other than intensity, the $\mathcal{P}_r$ probability densities can also model color, texture, or any other appearance features. In this paper, we focus on intensity-based $\mathcal{P}_r$; however, the algorithms we present can equally be used for all other appearance features. In the rest of the paper, we omit the geometry prior term in (9) by assuming uniform shape priors. A term that minimizes the boundary length (surface in 3D) frequently used in conventional level set based methods [38] or advanced shape priors [32] can easily be incorporated into the algorithms we present.

Note that the above DNLS-based energy formulation is for region-based image segmentation. Additionally, edge-based image segmentation methods that utilize image gradients in order to specify object boundaries are available in the literature. In this paper, we focus on region-based segmentation and show the two-phase and multiphase applications. However, the proposed DNLS can easily be formulated for (and applied to) edge-based segmentation. For instance, in an edge-based image segmentation using the proposed DNLS, the data term $\mathcal{P}(I/\mathbf{W})$ in equation (7) becomes the likelihood that the contour is on the image edge by first computing the image gradient.

IV. Two-Phase Segmentation

Segmentation of an image into two regions (foreground and background) with equation (9) can be accomplished by using a single level set function f. That is, $f > 0.5$ in the foreground and $f < 0.5$ in the background regions. In this two-phase case ($R = 2$), equation (9) can now be rewritten as

$$E(\mathbf{W}) = -\int_{\Omega} \left(f(\mathbf{x}) \log \mathcal{P}_f + (1 - f(\mathbf{x})) \log \mathcal{P}_b \right) \mathbf{dx} \quad (10)$$

where $\mathcal{P}_f$ and $\mathcal{P}_b$ are the pdfs in the foreground and background regions, respectively. To simplify the notation, we use $\mathcal{P}_f$ instead of $\mathcal{P}_f(I(\mathbf{x}), \mathbf{x})$. We also use f or $f(\mathbf{x})$ instead of $f(\mathbf{x}; \mathbf{W})$ for a similar reason. Since $f(\mathbf{x})$ is close to 1 inside the object and close to 0 outside, it acts as a Heaviside function. Hence, equation (10) gives the DNLS version of the general two-phase equation in (2).

Rearranging (10) (and ignoring the term that is not a function of the discriminant W), we get

$$E(\mathbf{W}) = -\int_{\Omega} \left(f(\mathbf{x}) (\log \mathcal{P}_f - \log \mathcal{P}_b) \right) \mathbf{dx} \quad (11)$$

The energy minimization implies computing the derivatives of equation (11) with respect to each discriminant parameter, w_{ijk}. During segmentation, the update to the discriminant weights, w_{ijk}, is obtained by minimizing the energy using gradient descent as

$$\frac{\partial E(\mathbf{W})}{\partial w_{ijk}} = -\left(\log \mathcal{P}_f - \log \mathcal{P}_b \right) \frac{\partial f(\mathbf{W})}{\partial w_{ijk}} \quad (12)$$

where

$$\begin{aligned} \frac{\partial f(\mathbf{W})}{\partial w_{ijk}} &= \frac{\partial}{\partial w_{ijk}} \left(1 - \prod_{r \in \aleph} (1 - g_r(\mathbf{x})) \right) \\ &= \left(\prod_{\substack{r \in \aleph \\ r \neq i}} (1 - g_r(\mathbf{x})) \right) \frac{\partial g_i}{\partial w_{ijk}} \\ &= \left(\prod_{\substack{r \in \aleph \\ r \neq i}} (1 - g_r(\mathbf{x})) \right) \left(1 - \prod_{l \neq j}^{M} \sigma_{il} \right) \frac{\partial \sigma_{ij}}{\partial w_{ijk}} \\ &= -\left(\prod_{\substack{r \in \aleph \\ r \neq i}} (1 - g_r(\mathbf{x})) \right) g_i(\mathbf{x}) (1 - \sigma_{ij}(\mathbf{x})) x_k \end{aligned} \quad (13)$$

Therefore, during the level set evolution, the discriminant parameters are updated on each iteration as $w_{ijk} \leftarrow w_{ijk} - \gamma \frac{\partial E}{\partial w_{ijk}}$, where γ is the step-size. Since the evolution of the proposed parametric level set is not constrained by the standard CFL condition, we can easily choose large γ at the beginning of the evolution and gradually decrease it as the segmentation progresses, for fast convergence. Notice that the level set function, f, remains regular throughout the evolution; hence, no re-initialization or additional regularizing term is needed.

1) Homogenous (Piecewise Constant) Case: Chan and Vese [38] (CV) proposed one of the most popular two-phase level set based segmentations by approximating the image into piecewise constant regions and evolving the level set in order to minimize the variance of each partition. In this case, since the image is assumed to be made up of two piecewise constant regions, a Gaussian probability density with fixed standard deviation and constant mean can be used for the $\mathcal{P}_f$ and $\mathcal{P}_b$ in equation (10). Hence, $\mathcal{P}_f \propto exp^{-\eta(I(\mathbf{x})-c_1)^2}$, and $\log \mathcal{P}_f(I(\mathbf{x}), \mathbf{x}) \propto -(I(\mathbf{x})-c_1)^2$. Therefore, the CV equivalent of the proposed DNLS two-phase piecewise constant region-based variational energy to be minimized is given as

$$E(\mathbf{W}) = \int_{\Omega} (I(\mathbf{x}) - c_1)^2 \; f(\mathbf{x}) + (I(\mathbf{x}) - c_2)^2 (1 - f(\mathbf{x})) d\mathbf{x} \quad (14)$$

where c_1 and c_2 are the mean intensities in the foreground and background regions, respectively. The average intensity in the foreground, c_1, can be obtained by

$$c_1(f) = \frac{\int_{\Omega} I(\mathbf{x}) H(f(\mathbf{x}) - 0.5) d\mathbf{x}}{\int_{\Omega} H(f(\mathbf{x}) - 0.5) d\mathbf{x}} \quad (15)$$

That is, the mean intensity in the foreground, c_1, is simply the average of the intensities of all the pixels where $f(\mathbf{x}) > 0.5$. Similarly, c_2 is given as

$$c_2(f) = \frac{\int_\Omega I(\mathbf{x})(1 - H(f(\mathbf{x}) - 0.5))d\mathbf{x}}{\int_\Omega (1 - H(f(\mathbf{x}) - 0.5))d\mathbf{x}} \tag{16}$$

2) Inhomogeneous (Piecewise Smooth) Case: During inhomogeneous image segmentation, the pdf at the foreground (and at the background) cannot be approximated by a constant mean Gaussian. Since the intensity inhomogeneity is usually due to a slowly varying field, in a small local region the intensity distributions can still be approximated by a constant mean Gaussian [22]–[24]. Therefore, the mean intensities c_1 and c_2 in equation (14) are now replaced by their localized versions $c_1(\mathbf{x})$ and $c_2(\mathbf{x})$. Following a similar approach proposed in [22] for localizing region-based energies in level set segmentation methods, we can write $c_1(\mathbf{x})$ and $c_2(\mathbf{x})$ as

$$c_1(f) = \frac{\int_\Omega B(\mathbf{x}, r) I(\mathbf{x}) H(f(\mathbf{x}) - 0.5)d\mathbf{x}}{\int_\Omega B(\mathbf{x}, r) H(f(\mathbf{x}) - 0.5)d\mathbf{x}} \tag{17}$$

$$c_2(f) = \frac{\int_\Omega B(\mathbf{x}, r) I(\mathbf{x})(1 - H(f(\mathbf{x}) - 0.5))d\mathbf{x}}{\int_\Omega B(\mathbf{x}, r)(1 - H(f(\mathbf{x}) - 0.5))d\mathbf{x}} \tag{18}$$

where $B(\mathbf{x}, r)$ is a local region mask of radius r. That is, $B(\mathbf{x}, r) = 1$ for all pixels that are at a radius of less than or equal to r from pixel $\mathbf{x}$, and $B(\mathbf{x}, r) = 0$ otherwise.

V. Multiphase Segmentation

In this section, we extend the DNLS framework to simultaneous segmentation of multiple regions, $R > 2$. The general segmentation equation in (9) can be directly used for multiphase image segmentation by employing R different level set functions, each representing one region. However, as noted in [4], [18], and, [20] the level set functions need coupling in order to avoid creation of overlaps (constraint of disjoint regions) and gaps (there must not be pixels that are not assigned to any region). To overcome this limitation, three major approaches are available in the literature.

The first approach is based on using one level set function for each region, together with a Lagrangian multiplier for a coupling force term that enforces the constraint of disjoint regions [16], [18]. However, this additional coupling term results in significant computational cost [4]. The second approach, proposed by Vese and Chan [20], uses $\log_2 R$ level sets to represent R regions. This approach naturally handles the constraint of disjoint regions without the need for any additional coupling term if the number of regions is a power of 2. The fact that the [20] method does not represent each object with its unique level set limits the suitability of the approach for certain applications (e.g., in applications that require tracking of the individual objects and (or) use of their shape priors). The third approach, proposed by Brox and Cremers [4], uses the concept of competing regions. By enforcing a competition between the level sets assigned to the different objects, the method avoids the creation of overlaps and gaps, without requiring the additional coupling force term. We use a method similar to the Brox-Cremers approach of competing regions, and propose an efficient DNLS-based multiphase segmentation framework, by starting from the energy maximization of equation (9).

Since the DNLS level set presented in section II is made up of the union of many polytopes, the single level set function given in equation (5) can be used to segment R regions. Each of the polytopes can individually be regarded as a level set function, and hence, each can be assigned to a different region (object). We represent each region, r, by a unique level set f_r, that is formed by the union of some of the polytopes of the function f. See Fig. 4(b) for an example of polytopes assigned to three different regions using random label assignment initialization, to create a unique level set f_r for each region.

We can use the energy given in equation (9), by omitting the geometry prior term using uniform shape priors assumption, for the multiphase segmentation

$$E(\mathbf{W}) = -\int_\Omega \sum_{r=1}^{R} f_r \log\ (\mathcal{P}_r)\mathbf{dx} \tag{19}$$

However, since $\log\ (\mathcal{P}_r)$ is always negative, during minimization of the energy in equation (19) all the f_r level sets quickly become zero, resulting in the disappearance of all the regions, $\mathbf{\Omega}_r$. By comparison, the energy for the two-phase case in equation (11) has two competing regions all the time. That is, the $\log \mathcal{P}_f$ at the foreground is balanced by the $-\log \mathcal{P}_b$ at the background. There is no such balancing term in equation (19) for the multiphase case. Therefore, we can introduce a similar concept of competing regions in the multiphase equation. Hence, the energy to be minimized can be given as

$$E(\mathbf{W}) = -\int_{\mathbf{x}\in\Omega} \sum_{r=1}^{R} f_r \left(\underbrace{\log \mathcal{P}_r - max_{t\neq r} \log \mathcal{P}_t}_{S(\mathbf{x},r)} \right) \mathbf{dx} \tag{20}$$

Let us look at the sign of $S(\mathbf{x}, r)$. $S(\mathbf{x}, r)$ is positive for the level set with the best pdf $\mathcal{P}_{rb}$, and negative for all the other level level sets, $\mathcal{P}_r$. $\mathcal{P}_{rb}$ is the best pdf at pixel location $\mathbf{x}$ with intensity $I(\mathbf{x})$, if

$$\mathcal{P}_{rb}(I(\mathbf{x}), \mathbf{x}) > \mathcal{P}_r(I(\mathbf{x}), \mathbf{x}), \quad \forall r \in \{1, ..., R\}, \text{ and } rb \neq r. \tag{21}$$

Therefore, based on the sign of $S(\mathbf{x}, r)$, the level set with the best pdf, f_{rb}, at a given pixel location $\mathbf{x}$ advances to include the pixel; whereas, all the other level sets f_r retreat to exclude the pixel. For example, from Fig. 4(d) the green and yellow level sets retreat to exclude the pixel $\mathbf{x}$, and the red level set advances to include the pixel. That is, in (20) at each pixel location we maximize the most likely pdf (the object label that can best explain the intensity at that location), while at the same time we minimize all the other pdfs. Maximizing the pdf of only one level set at each location ensures that every pixel has exactly one level set (label) assigned to it. Therefore, no gaps or overlaps are created when (20) is minimized for the multiphase segmentation. During segmentation, the energy is minimized using gradient descent by computing the derivatives of equations (20) with respect to each discriminant parameter, w_{ijk}.

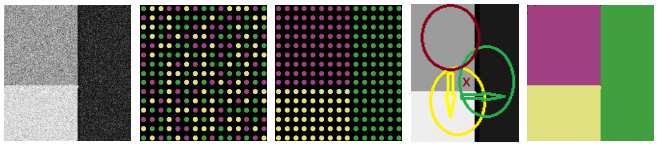

Fig. 4. a) Multiphase image. b) and c) show the effect of applying the labeling energy term, E_L (polytopes assigned to the same region label are shown with the same color). d) shows the effect of the deformation term, using enlarged polytopes for clarity, and the arrows show the direction of their deformation. e) Final segmentation result.

The sign of $S(\mathbf{x}, r)$ in equation (20) determines the direction of movement of the level set; that is, whether a given level set, f_r advances to include a given pixel or retreats to exclude the pixel. The magnitude of $S(\mathbf{x}, r)$ gives how fast the level sets move. If we simply use the sign of $S(\mathbf{x}, r)$ (hence, force all the level sets to move at the same rate), then (20) can be simplified to give

$$E(\mathbf{W}) = \int_{\mathbf{x}\in\Omega} \left(-f_{rb} + \sum_{\substack{r=1 \\ r\neq rb}}^{R} f_r \right) \mathbf{dx} \tag{22}$$

3) Homogenous (Piecewise Constant) Case: Next, we discuss the case of piecewise constant (homogenous) image segmentation. Since the image is assumed to be made up of R piecewise constant regions, a Gaussian probability density with fixed standard deviation and constant mean can be used for $\mathcal{P}_r$. Hence, $\mathcal{P}_r \propto exp^{-\eta(I(\mathbf{x})-c_r)^2}$, and $\log \mathcal{P}_r(I(\mathbf{x}), \mathbf{x}) \propto -(I(\mathbf{x}) - c_r)^2$. Therefore, following equation (21) the best pdf, $\mathcal{P}_{rb}$, at location $\mathbf{x}$ is now the r label that results in the smallest $(I(\mathbf{x}) - c_r)^2$.

In a piecewise constant case (homogenous image), the DNLS provides an additional benefit, which we discuss next. Using DNLS, where a given unique level set is created by assigning different labels to the different polytopes, the movement of the surfaces between the different objects can take place in two ways: by the deformations of the polytopes, and by a change in the labels of the polytopes. The DNLS multiphase total energy can then be given as $E_T = E_L + E_D$; where E_L is the energy for changing the labels of the polytopes, and E_D is the energy for deforming the polytopes. This makes the proposed DNLS-based multiphase algorithm computationally even more efficient, and also makes it less sensitive to initialization.

The deformation term E_D is the same as the energy given in (22), except that we can now consider only the polytopes that are in the immediate neighborhood of the pixel, $i \in \aleph(\mathbf{x})$. That is, large surface movement and initialization are handled by the E_L term, and local deformation is handled by the E_D term. Hence, equation (22) becomes

$$E_D(\mathbf{W}) = \int_{\mathbf{x}\in\Omega} \left(-f_{rb} + \sum_{\substack{i=1 \\ i\notin rb \\ i\in\aleph(\mathbf{x})}}^{N} f_i \right) \mathbf{dx} \tag{23}$$

That it, only the polytopes in the immediate neighborhood of the pixel will advance or retreat to include or exclude the pixel. Therefore, the energy in equation (23) becomes minimum when the polytopes that are part of the best pdf level set label, rb, include the pixel at $\mathbf{x}$, and all the remaining polytopes in the neighborhood with other labels exclude that pixel. Since we look at only a fixed number of neighboring polytopes at each pixel, the computational time of the E_D term is independent of the number of regions R to be simultaneously segmented.

Algorithm 1 Algorithm for Multiphase Image Segmentation

Input: The image to be segmented, parameters N, M, gradient step size γ, and total number of iteration T

Output: The final segmented image and its discriminants $\mathbf{W_f}$

Initialization :

1: Get the initial discriminant parameters $\mathbf{W}$ using (6)
2: Assign region label for every polytope. This label initialization, L, can be assigned randomly.

LOOP Process

3: **for** *iteration* $t = 0$ to $t = T$ **do**
4: Step 1: minimize E_L given in (24) to change the labels of the polytopes (new $\mathbf{L}$)
5: Step 2: minimize E_D given in (23) using gradient descent to segment the images by deforming the polytopes $w_{ijk} \leftarrow w_{ijk} - \gamma \frac{\partial E_D}{\partial w_{ijk}}$
6: **end for**
7: **return** Final weights $\mathbf{W_f}$ and polytopes label set $\mathbf{L}$
8: Get the final multiphase segmented image: from the $\mathbf{W_f}$ using (5), and from the final labels of the polytopes $\mathbf{L}$.

For the label assignment energy term E_L, we use a simple K-means clustering; however, any advanced clustering method can be employed. By first computing the mean intensities for each polytope p_i, we can cluster them into R region labels. That is, given a set of N polytopes with their average intensities $(p_1, p_2, ..., p_N)$, k-means clustering aims to partition the N polytopes into R region label sets $\mathbf{L} = \{L_1, L_2, ..., L_R\}$ to minimize the within-cluster sum of squares as

$$E_L = \underset{\mathbf{L}}{\operatorname{argmin}} \sum_{r=1}^{R} \sum_{p\in L_r} (p - c_r)^2 \tag{24}$$

where c_r is the mean intensity of all the polytopes assigned to region r (the mean intensity of region r). The E_L energy becomes minimum when the polytopes with closer mean intensity values are labeled similarly. For instance, Fig. 4 (c) shows the effect of applying E_L to (b), which changes the label assignments of the polytopes. Fig. 4(e) shows the final result using both the E_L and E_D terms. The summary of the proposed multiphase segmentation of homogenous image is given in Algorithm 1.

a) Computational cost: The computational cost of K-means clustering is proportional to both the number of data points N (polytopes) and the number of clusters R (regions). The number of polytopes we use, N, is fixed and is independent of the number of regions R to be simultaneously segmented. As shown in the experiment section VI-A,

$N = 100$ polytopes are usually enough for a smooth representation of shapes. Therefore, the E_L term due to clustering of 100 polytopes (data points) is computationally insignificant compared to the gradient decent based E_D term. Since the computational time of the E_D term is independent of the number of regions R to be simultaneously segmented, the increase in the computational cost due to the increase in the number of regions R comes only from the clustering part. Since the clustering of around $N = 100$ polytopes takes insignificant time (compared to the E_D gradient descent term), the overall computational time of our multiphase algorithm remains almost constant as the number of regions R to be segmented grows.

4) Inhomogeneous (Piecewise Smooth) Case: For multiphase segmentation of inhomogeneous images, a similar local region-based segmentation approach discussed in section IV-.2 can be used together with equation (20). That is, the mean intensity c_r for each region, r, is now replaced by its localized versions $c_r(\mathbf{x})$. However, computation of $c_r(\mathbf{x})$ for each local region using convolution is computationally expensive [22]. Luckily, our DNLS formulation allows an efficient way of computing local mean statistics because of its use of polytopes. The mean intensity for each polytope p_i is obtained automatically during the f function evaluation, with no additional computational expense. Therefore, the mean local intensity for region r, $c_r(\mathbf{x})$, can now be obtained by simply averaging the mean intensities of the polytopes in the neighborhood. It is important to notice that the quality of any local region-based image segmentation depends heavily on the size of the local region chosen [22], that is, on the radius, rad, of the local ball size, $B(\mathbf{x}, rad)$. Therefore, the ability to efficiently compute local region statistics at multiple local region sizes is crucial. Since the proposed DNLS framework allows obtaining these local region statistics using the polytopes with little additional computational expense, we can easily obtain and use these statistics at multiple local region sizes.

VI. Experiments

In this section, we present the results of seven experiments. In section VI-A, we present the effect of the DNLS shape representation parameters (N and M) on the segmentation quality and computational time. In Section VI-B, we show the segmentation results of our DNLS on two-phase images. In this section, we also compare our method with the conventional region-based level set method of Chan and Vese (CV) [38]. In Section VI-C, we evaluate the effect of noise (at different levels) on the segmentation performance by comparing our DNLS method with the CV method. In Section VI-D, we compare our DNLS with three different state-of-the-art level set methods on large data set corrupted with Gaussian, Poisson, Speckle, and Salt & pepper noise types. We give a brief comparison of our DNLS with the Bernard *et al.* [3] parametric level set in section VI-E. In Section VI-F, we compare the proposed DNLS multiphase version with the CV multiphase [20] for a piecewise constant image segmentation. In this section, we focus on the effect of initialization, and the growth in computational time as the number of objects to be simultaneously segmented increases. Finally, in section VI-G, we provide some segmentation results for inhomogeneous images. Our algorithm is implemented in C++ using the Insight Segmentation and Registration Toolkit (ITK) [39] on 2.5-GHz Intel Core i7, 8 GB RAM machine. For comparisons of the homogenous image segmentation, we use the optimized implementations of the two-phase and multiphase CV level sets available in the latest ITK. We use a Matlab implementation for comparison with the other level set methods [3], [14], [15] in Sections VI-D and VI-E, since these level set methods have publicly available Matlab implementations (mostly by the corresponding authors).

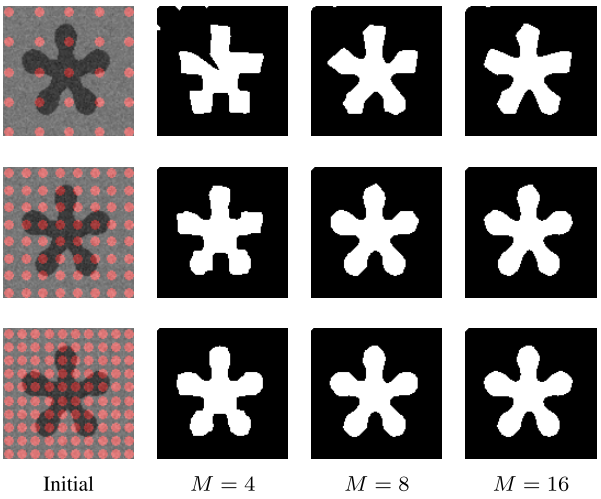

Fig. 5. Demonstration of the effect of the number of polytopes and the number of discriminants of the DNLS on the segmentation accuracy. Top to bottom rows correspond to N = 25, 64, and 100, respectively. The left column shows the initialization. Columns 2 to 4 (left to right) correspond to M = 4, 8, and 16, respectively.

A. The Effect of the DNLS Shape Representation Parameters

The DNLS shape representation equation (5) has two parameters that control the smoothness of the shape model: the number of polytopes, N, and the number of discriminants per polytopes, M. Here we investigative the effects of N and M on the segmentation accuracy and the computational time. Figure 5 shows the segmentation of an artificial image with varying numbers of polytopes (N) and discriminants (M). As can be seen from the figure, a smooth and accurate DNLS shape representation can be achieved by increasing the number of polytopes (N) and (or) by increasing the discriminants per polytope (M). Increasing these parameters results in an increase in computational cost. However, there is an upper limit on the M and N parameters after which any further increase in their values does not result in any meaningful gain in accuracy, as can also be seen from Table I. For instance, in Fig. 5 there is no noticeable accuracy difference by using $N = 64$ with $M = 8$, or by using $N = 100$ with $M = 16$.

Table I shows both the CPU time (T in seconds) required and the DICE coefficient (DC in %) [40] of the segmentation results for images shown in Fig. 5. We can see from the table that the rate at which the CPU time increases as the N and M parameter values increase is relatively small. This is mainly because although a single iteration now takes longer time, the segmentation converges faster and hence fewer iterations

TABLE I

QUANTITATIVE EVALUATION OF THE EFFECT OF N AND M PARAMETERS (PAR.) FOR IMAGES IN FIG. 5. DICE (DC) IN % AND TIME (T) IN SECONDS

Par.	M=4		M=8		M=16	
	DC	T	DC	T	DC	T
N=25	89.68	0.073	95.31	0.097	96.00	0.113
N=64	95.57	0.093	**98.02**	0.110	**98.59**	0.130
N=100	97.23	0.107	**98.57**	0.127	**98.91**	0.150

are required as the N and M parameter values increase. In addition, since we use only a fixed number of neighboring polytopes at each pixel point (as discussed in section II), the increase in N has less effect on the CPU time. In the rest of the experiments, we use $N = 100$ and $M = 16$ values, unless explicitly specified.

B. Two-Phase Segmentation Results

Figure 6 shows segmentation results of four two-phase images using DNLS (second column) and CV (third column) [38] methods. For both DNLS and CV, we used a regularly distributed initialization similar to the one shown in Fig. 5, with $N = 100$ and $M = 16$. For the CV method, the use of regularly distributed level sets is suggested in [20] and [41] as a better initialization for good segmentation quality and reduced computational time. As can be seen from Fig. 6, the proposed DNLS results in better (clean) segmentation compared to the CV method. We tune the smoothness term (length constraint) of the CV method to obtain the highest possible DICE score for the results in Fig. 6. By using a larger smoothness coefficient (larger penalty for the length of the contour), some of the tiny noisy fragments can be removed; however, a large increase in the smoothness coefficient makes the contour stiff and decreases the overall DICE score. On the other hand, the proposed DNLS results are free from any tuning of the smoothness term or parameter (since large enough N and M values can be chosen and fixed for all the images, as discussed in Section VI-A).

In addition, DNLS achieves these results at a much smaller computational time. Table II shows both the CPU time required and the DICE score of the segmentation results for images shown in Fig. 6. The computational time for the CV level set is shown for both the dense and the sparse implementations available in ITK [39]. It can be seen from the table that DNLS achieves equivalent or better DICE scores with a computational speed of around 10 times compared to even the fastest sparse implementation of the CV method. Notice that two-phase images can have multiple objects as long as all the objects have the same phase (intensity level), as can be seen in columns (a) and (b) of Fig. 6.

C. The Effect of Noise Level on the Segmentation

In Fig. 7, we compare the segmentation performance of the proposed DNLS with CV method in the presence of various amounts of additive Gaussian noise. The first row in Fig. 7 shows the synthetic image with noise levels of 80, 100, 120, 140, and 160 standard deviations (SD) from

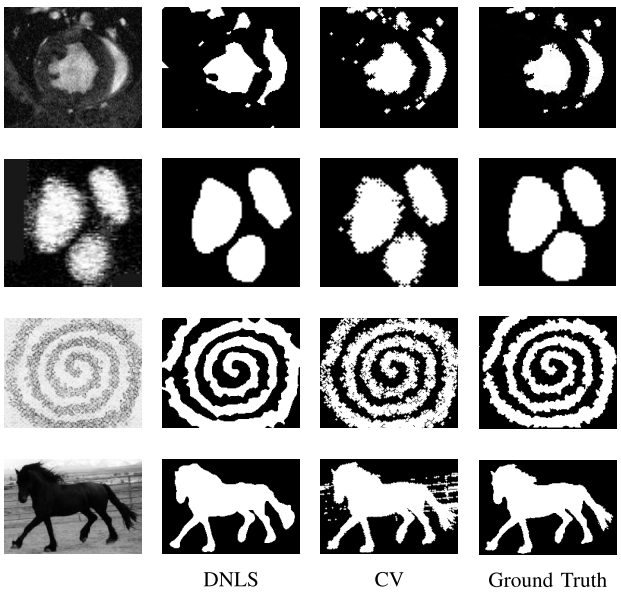

Fig. 6. On the first column (left) are the images to be segmented. The second column gives the segmentation results using the proposed DNLS. The third column gives the results obtained using the CV method, and the last column is the ground truth segmentation result.

TABLE II

QUANTITATIVE COMPARISON OF DNLS AND CV METHODS FOR IMAGES IN FIG. 6. IM1 TO IM4 DENOTE IMAGES ON FIRST TO LAST ROW, RESPECTIVELY. DICE (DC) IN % AND TIME (T) IN SECONDS

	CV Dense		CV Sparse		DNLS	
	DC	T	DC	T	DC	T
IM1	98.2	10.2	98.1	1.91	**98.4**	**0.19**
IM2	93.3	2.82	93.2	0.53	**95.1**	**0.05**
IM3	87.4	15.3	87.2	2.90	**90.2**	**0.31**
IM4	87.1	29.9	87.0	5.63	**96.4**	**0.40**

left to right (columns). The original image has an intensity range between 0 and 250. For the CV level set, we choose the smoothness coefficient that gives the best DICE score. A larger smoothness coefficient can be used to get results with less noisy fragments; however, as the smoothness coefficient increases, the contours become too stiff and reduce the DICE score. It is clear from the figure that the proposed DNLS method is less sensitive to noise and it has a smoothing property. This is mainly because the polytopes in the DNLS cannot capture extremely tiny fragments such as noise blobs of a radius less than 2 pixels. Note that no internal energy term (that controls the length of the contour) is used in our DNLS to generate the results, as mentioned in section III.

In Fig. 8, we give a quantitative comparison of the DNLS (solid line) and the CV method (dashed line) at varying noise levels for the image shown in Fig. 7. The figure shows the robustness of the proposed DNLS method when segmenting noisy images.

D. Comparison of Different State-of-the-Art Level Set Methods on Large Dataset With Four Noise Types

In this section, we compare the performance of the DNLS with three other popular level set based segmentation techniques using walking person data set (obtained from [41].

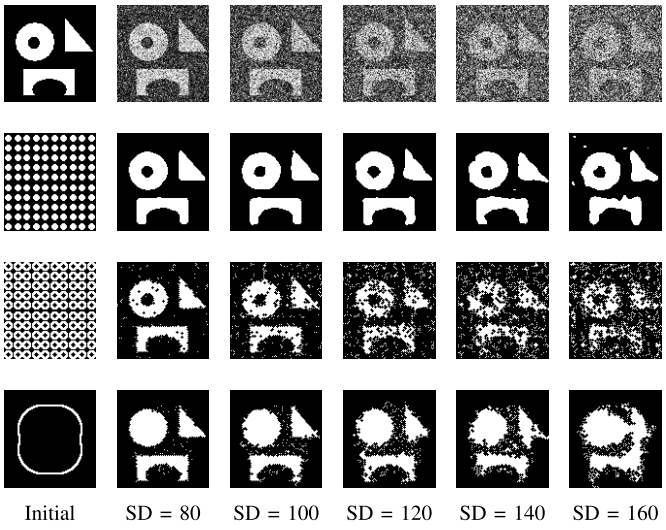

Fig. 7. On the first row are images with varying noise levels. The second row shows the segmentation results using the proposed DNLS method. The third and fourth rows give the results using the conventional CV method, with the different initializations shown on the first columns of both rows.

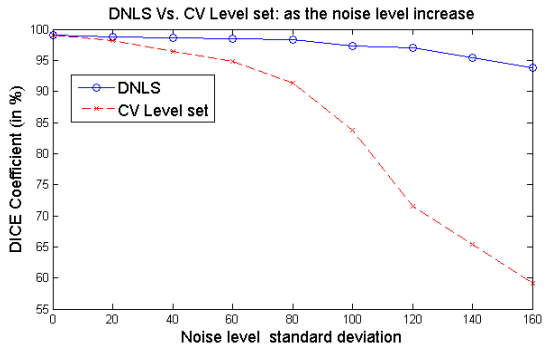

Fig. 8. Demonstration of the effect of noise level on the segmentation quality. Comparison of the DNLS with the conventional level set method. Regularly distributed initialization is used for both methods.

The three level sets methods we use for comparison are CV by Chen and Vese [38], DRLSE by Li *et al.* [14], and RD method by Zhang *et al.* [15]. We add four different noise types: Gaussian, Poisson, Speckle, and Salt & pepper to the images in order to compare the performance of the different level sets. Figure 9 shows an example of the four noise types and their corresponding segmentation using the different level set methods. From the figure it is clear that the RD method [15] and our DNLS have less sensitivity to noise.

Table III shows the average CPU time per image and the average DICE score of the segmentation results of the four different level set methods using fifty walking person images [41] corrupted with four different noise types. The table shows the proposed DNLS has the least sensitivity to noise while also having the smallest computational time compared to all the other three level set methods. We used publicly available Matlab implementations of CREASEG [42] for the Chen and Vese [38] and DRLSE [14] methods, and code shared online by the authors of RD method [15].

Note that, the DRLSE [14] and RD [15] methods have relatively fast evolution and are robust to noise compared to

TABLE III

QUANTITATIVE COMPARISON OF FOUR LEVEL SET METHODS WITH DIFFERENT NOISE TYPES. AVERAGE DICE (DC) IN % AND AVERAGE TIME (T) IN SECONDS

	Poisson		Gaussian		Speckle		Salt&Pepper	
	DC	T	DC	T	DC	T	DC	T
CV	98.3	6.43	88.3	6.27	87.6	6.51	89.4	6.07
DRLSE	98.4	4.21	90.1	4.53	88.2	4.60	90.6	4.37
RD	**98.7**	3.03	92.2	3.34	91.4	3.42	92.8	3.14
DNLS	98.5	**0.92**	**94.6**	**0.95**	**93.8**	**0.97**	**94.7**	**0.94**

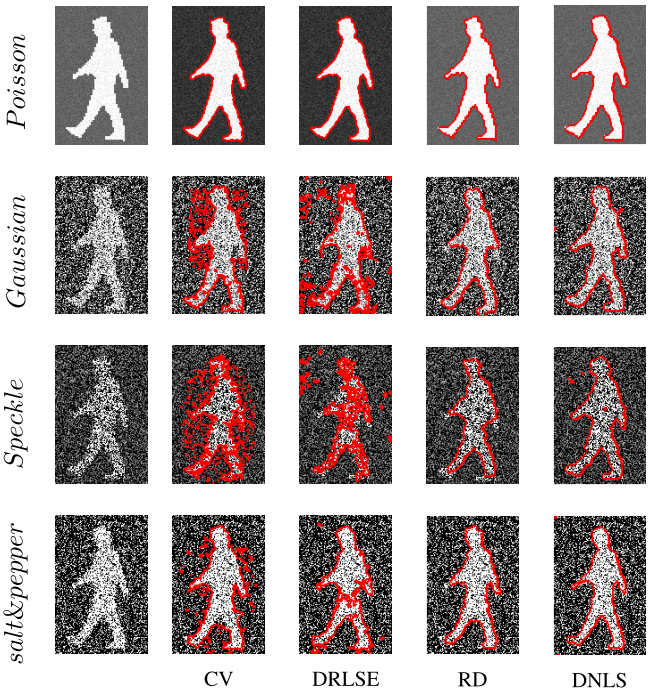

Fig. 9. Comparison of segmentation results using four different level set methods on image corrupted by four noise types.

the original (direct application) of level set method. However, DRLSE and RD methods, like all the other non-parametric level set methods, represent contours by embedding them in a higher dimensional space (for instance a signed distance function) which results in higher computation time. On the other hand, our DNLS uses a parametric shape representation which only needs a limited number of parameters to represent any shape (and hence decreases the dimension of the problem) resulting in significantly reduced computation time. In addition, in order to handle noise corruption, DRLSE and RD methods still require tuning of parameters. For instance, choosing larger weight for the boundary length term can make the contours stiff resulting in lack of flexibility to handle complex shapes, while choosing smaller weight results in fitting of the contours to noise fragments. In comparison, our DNLS handles significant noise corruption without the need for using the length term or any parameter tuning.

E. Comparison With Other Parametric Level Set Method

In Fig. 10, we show some segmentation comparisons of the proposed DNLS with B-spline based parametric level set method of Bernard *et al.* [3]. We use CREASEG [42], which

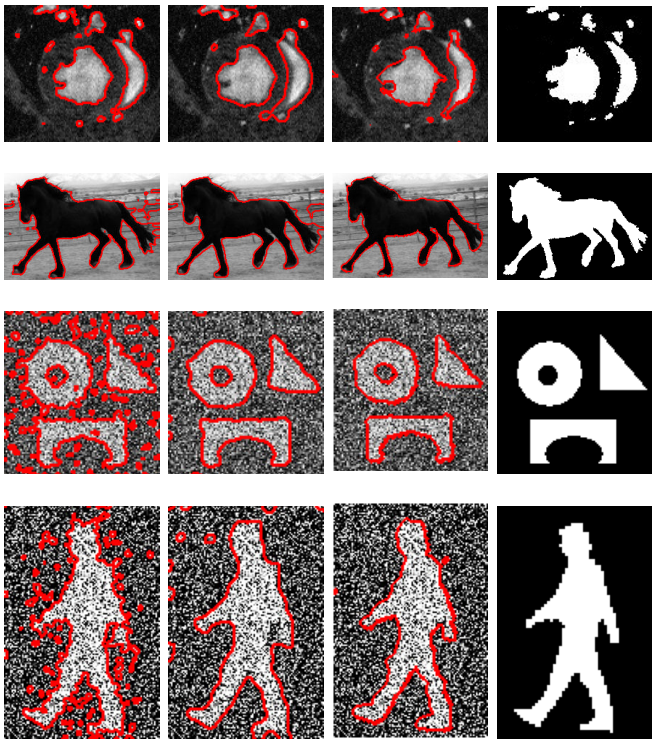

Fig. 10. Segmentation using the Bernard et. al. [3] parametric level set with $h = 1$ on the first column (left) and with $h = 2$ on the second column. Third column gives segmentation using DNLS, and ground truth segmentation on the last column (right).

is a publicly available Matlab implementation of [3]. The B-spline coefficient parameter h determines the smoothness of the Bernard *et al.* [3] segmentation. We can see from the figure that $h = 1$ results in noisy segmentation. On the other hand, $h = 2$ can be too strong and limits the smoothness of the segmentation, which can be seen from Fig. 10 horse and walking person segmentations. For instance, with $h = 2$ we can see the inability of the contour to get between the two back legs of the horse and back hand of the person. Note that h can only be an integer in [3], hence we cannot choose an intermediate value to get better results. On the other hand, the proposed DNLS parametric level set method has a good balance of smoothness and gives better segmentation, as can be seen from Fig. 10 and Table IV. From Table IV, we can also see that DNLS achieves better segmentation results in less computational time compared to the Bernard *et al.* [3]. In addition, DNLS does not require tuning of the smoothness parameters for every image (since a large enough number of polytopes N and discriminants M can be chosen and fixed, as discussed in Section VI-A). It should be noted that both the Bernard *et al.* [3] method (with the proper choice of the smoothness parameter) and our DNLS are less sensitive to noise compared to the conventional non-parametric level set methods. This can be seen by comparing the segmentation results of the noisy image in Fig. 10 third and fourth rows with that of Fig. 7 and Fig. 9. However, unlike the proposed DNLS method, the parametric level set of Bernard *et al.* [3] requires re-normalization of the level set function during the evolution process. In addition, [3] has the same drawbacks as the conventional (nonparametric) level set methods when applied to multiphase and local region-based image segmentations.

TABLE IV

QUANTITATIVE COMPARISON OF DNLS AND BERNARD *et al.* [3] METHODS FOR IMAGES IN FIG. 10. IM1 TO IM4 DENOTE IMAGES FROM TOP TO BOTTOM ROWS IN THE FIGURE, RESPECTIVELY. DICE (DC) IN % AND TIME (T) IN SECONDS

	Bernard $h = 1$		Bernard $h = 2$		DNLS	
	DC	T	DC	T	DC	T
IM1	96.2	3.21	96.5	3.15	**98.4**	**0.76**
IM2	90.3	6.82	92.2	6.55	**96.3**	**1.40**
IM3	83.4	4.31	94.8	3.89	**95.7**	**0.78**
IM4	87.1	3.94	90.3	3.64	**94.4**	**0.95**

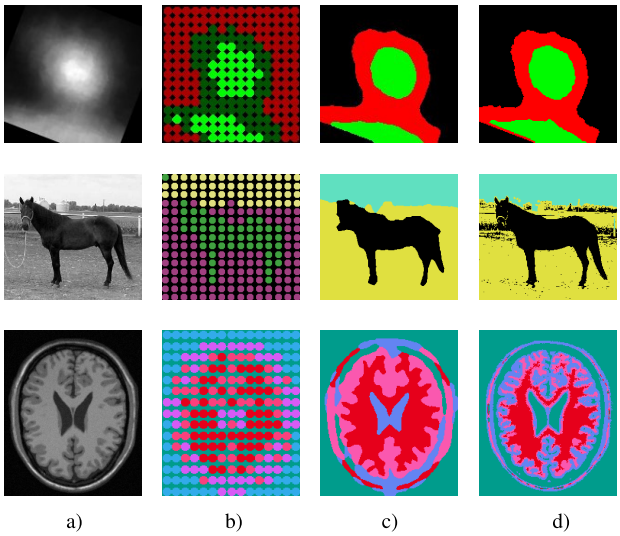

Fig. 11. Column (a) shows the images to be segmented, column (b) gives the multi-Otsu initialization used, column (c) shows the segmentation using DNLS-multiphase, and column (d) gives the result using the CV-multiphase method.

F. Multiphase Segmentation Results

In this section, we present the results of two experiments. In the first experiment, we present the effect of initialization using three images shown in Fig. 11 column (a), and compare the performances of the proposed DNLS-multiphase with the standard CV-multiphase level set [20]. Figure 11 shows the segmentation results using a multi-Otsu threshold method [43] to first obtain good initialization. As can be seen from the figure, both the proposed DNLS and CV-multiphase methods give good comparable segmentations (except for the horse image where the CV-multiphase resulted in noisy segmentation). However, good initialization using methods such as multi-Otsu is computationally expensive and less robust as the number of phase increases. Therefore, it is crucial to have a multiphase segmentation method that is less sensitive to initialization.

Figure 12 gives the segmentation comparison of DNLS-multiphase and the CV-multiphase when random internalization is used. It can be seen from Fig. 12 that when the level sets are randomly initialized, the CV-multiphase level set frequently converges to bad segmentation; whereas, our DNLS-multiphase still converges to a good segmentation.

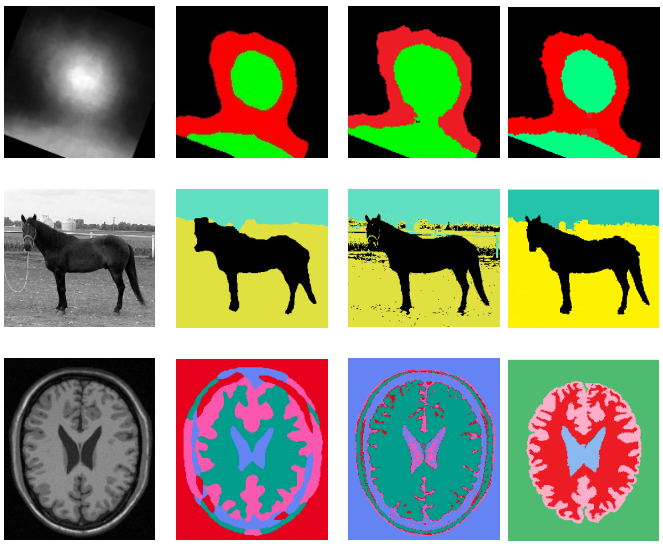

a) b) c) d)

Fig. 12. Comparison of the DNLS-multiphase segmentation results on column (b), with the CV-multiphase result on column (c), using a random initialization. Column (d) shows the ground truth segmentation.

TABLE V

QUANTITATIVE COMPARISON OF DNLS AND CV METHODS FOR IMAGES IN FIG. 11 AND FIG. 12. IM1 TO IM3 DENOTE IMAGES ON THE FIRST TO THIRD ROW IN THE FIGURES, RESPECTIVELY. WE CONSIDER BOTH THE RANDOM AND OTSU INITIALIZATIONS. DICE (DC) IN % AND TIME (T) IN SECONDS

	DNLS-Otsu		CV-Otsu		DNLS-Random		CV-Random	
	DC	T	DC	T	DC	T	DC	T
IM1	**96.3**	**1.8**	94.2	21.9	**96.1**	**2.3**	83.1	25.3
IM2	**94.5**	**2.5**	89.2	26.7	**94.3**	**2.9**	88.7	28.2
IM3	90.7	**2.6**	**91.5**	31.5	**86.3**	**2.7**	78.4	35.7

Because of the label assignment energy term discussed in section V-.3, the proposed DNLS-multiphase is less sensitive to initialization, when compared to the CV-multiphase level set.

Note that for the brain MRI image segmentation, the nonbrain structures (the outer circular ring) surrounding the brain tissues are classified wrongly by both the CV-multiphase and our DNLS-multiphase methods in both Fig. 11 and Fig. 12. However, these nonbrain structures are usually removed by using simple techniques such as [44] before starting segmentation of brain tissues. Therefore, by using a preprocessing step to first remove the nonbrain structures, the proposed DNLS-multiphase can easily give a good segmentation of the brain tissues, even if random initialization is used.

Table V shows both the CPU time required and the DICE score of the segmentation results for images shown in Fig. 11 and Fig. 12. It can be seen from the table that DNLS-Multiphase achieves better DICE scores (except for the brain image with multi-Otsu initialization) with a much lower computational time compared to CV-multiphase [20]. For all the multiphase experiments we used $N = 225$ polytopes. Note that using even larger number of polytopes can help improve the quality of the brain image (which has very fine details)

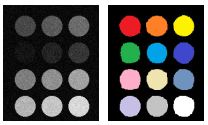

Fig. 13. Multiphase example (left) and segmented result (right).

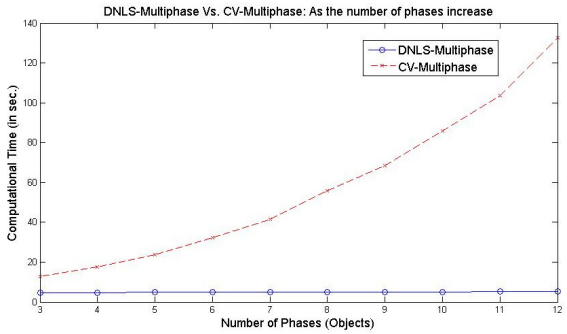

Fig. 14. Computation time as a function of the number of objects to be segmented.

segmentation, at the expense a slight increase in computational cost.

In the second experiment, we show the effect of the number of objects (phases) to be segmented on the computation time. For this purpose, we generate phantom images with various numbers of object phases; one example with 12 objects is shown in Fig. 13. Figure 14 shows the computation time as a function of the number of objects (with different phases) in the images: using the CV-Multiphase with sparse implementation (dashed line), and using the DNLS-multiphase (solid line). The time in the graph is obtained with similar segmentation quality of around 98.5% in DICE. The graph shows that the proposed DNLS-Multiphase requires an almost constant computation time independent of the number of objects to be segmented. The memory required also remains constant (not shown in the graph) in the proposed DNLS-multiphase, because the number of polytopes is fixed, and only their labeling changes as the number of objects in the image increases.

G. Inhomogeneous Image Segmentation Results

Finally, we show results of local region-based segmentation for inhomogeneous images. Figure 15 gives the segmentation of inhomogeneous images using the proposed DNLS local region-based method. Figure 15 column (a) shows the original homogenous images; column (b) shows the bias field added to the images on column (a) to obtain the inhomogeneous images shown on column (c). Column (d) shows the final segmented images using the proposed DNLS local region-based method for the inhomogeneous images of column (c). The figure gives the segmentation results for both two-phase (on the first two rows) and multiphase (the bottom row) piecewise smooth images.

It should be noted that, in local-region based segmentation, the size of the local region considered and the initialization have significant impact on the quality of the segmentation. The radius of the local region chosen determines how local the resulting segmentation will be, and hence it should be chosen

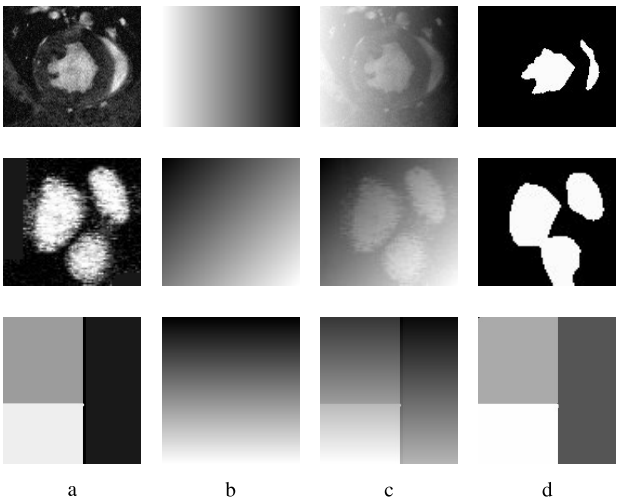

Fig. 15. Inhomogeneous image segmentation using DNLS.

based on the scale of the object of interest and properties of the surrounding area [22]. In Figure 15, we tune the radius parameter to get good results (radius ranging from 5 to 15 pixels are tested,and the results in the figure are generated with pixel radius of 10). In addition, the *inhomogeneous* image segmentation using the proposed method is sensitive to initialization (similar to the other level set based methods in the literature). On the other hand, the *homogenous* version of our DNLS is less sensitive to initialization due to the fact that we use clustering of the polytopes as part of the energy. But for inhomogeneous images, we can not cluster the polytopes by using a simple K-means, hence our level set acts similarly to the conventional level set method in terms of sensitivity to initialization. We refer the reader to Lankton and Tannenbaum [22] for an extensive discussion of the challenges of local-region size and initialization for inhomogeneous image segmentations.

VII. Conclusion

In this paper, we presented a novel parametric level set method that naturally keeps the level set function regular all the time, and that does not need any form of re-initialization or the use of any regularizing term. Due to its parametric nature, the DNLS method also reduces the dimensionality of the problem, and its time step is not limited by the standard CFL condition, resulting in much faster computational speed. The proposed DNLS is also less sensitive to noise. In addition, we presented the DNLS-multiphase framework for simultaneous segmentation of multiple objects. The proposed DNLS-multiphase approach has the highly desired properties that it is less sensitive to initialization, and its computational cost and memory requirement remain almost constant as the number of objects to be segmented grows, while also representing each object with a unique level set. We formulated the segmentation algorithm in a Bayesian framework and used a variational approach to minimize the energy with respect to the discriminant parameters of the model. The proposed DNLS can be considered as an open framework that can be used with different active contour methods, and it also allows the use of different appearance models and shape priors. Although we have shown the application of our algorithm using only intensity, other descriptors such as texture, color, and motion vectors also can be used with the proposed segmentation method. The DNLS also has unique location information (due to its use of polytopes and discriminants) that can be used for powerful local appearance modeling and for local region-based segmentation of inhomogeneous images.

References

[1] S. Osher, "Fronts propagating with curvature-dependent speed: Algorithms based on hamilton-jacobi formulations," *J. Comput. Phys.*, vol. 79, no. 1, pp. 12–49, 1988.

[2] C. Li, C. Xu, C. Gui, and M. D. Fox, "Level set evolution without re-initialization: A new variational formulation," in *Proc. IEEE Comput. Soc. Conf. Comput. Vis. Pattern Recognit. (CVPR)*, vol. 1. Jun. 2005, pp. 430–436.

[3] O. Bernard, D. Friboulet, P. Thevenaz, and M. Unser, "Variational B-spline level-set: A linear filtering approach for fast deformable model evolution," *IEEE Trans. Image Process.*, vol. 18, no. 6, pp. 1179–1191, Jun. 2009.

[4] T. Brox and J. Weickert, "Level set segmentation with multiple regions," *IEEE Trans. Image Process.*, vol. 15, no. 10, pp. 3213–3218, Oct. 2006.

[5] S. Geman and D. Geman, "Stochastic relaxation, Gibbs distributions, and the Bayesian restoration of images," *IEEE Trans. Pattern Anal. Mach. Intell.*, vol. 6, no. 6, pp. 721–741, Nov. 1984.

[6] D. Mumford and J. Shah, "Optimal approximations by piecewise smooth functions and associated variational problems," *Commun. Pure Appl. Math.*, vol. 42, no. 5, pp. 577–685, 1989.

[7] T. Brox and D. Cremers, "On the statistical interpretation of the piecewise smooth mumford-shah functional," in *Proc. Int. Conf. Scale Space Variational Methods Comput. Vis. (SSVM)*, vol. 4485. May 2007, pp. 203–213.

[8] S. C. Zhu, T. S. Lee, and A. L. Yuille, "Region competition: Unifying snakes, region growing, energy/Bayes/MDL for multi-band image segmentation," in *Proc. 5th Int. Conf. Comput. Vis.*, Jun. 1995, pp. 416–423.

[9] J. A. Sethian, "A fast marching level set method for monotonically advancing fronts," *Proc. Nat. Acad. Sci. USA*, vol. 93, no. 4, pp. 1591–1595, 1996.

[10] R. T. Whitaker, "A level-set approach to 3D reconstruction from range data," *Int. J. Comput. Vis.*, vol. 29, no. 3, pp. 203–231, 1998.

[11] Q. Duan, E. D. Angelini, and A. F. Laine, "Real-time segmentation by active geometric functions," *Comput. Methods Programs Biomed.*, vol. 98, no. 3, p. 223– 230, 2010.

[12] A. Aghasi, M. Kilmer, and E. L. Miller, "Parametric level set methods for inverse problems," *SIAM J. Imag. Sci.*, vol. 4, no. 2, pp. 618–650, 2011.

[13] V. Estellers, D. Zosso, R. Lai, S. Osher, J. P. Thiran, and X. Bresson, "Efficient algorithm for level set method preserving distance function," *IEEE Trans. Image Process.*, vol. 21, no. 12, pp. 4722–4734, Dec. 2012.

[14] C. Li, C. Xu, C. Gui, and M. D. Fox, "Distance regularized level set evolution and its application to image segmentation," *IEEE Trans. Image Process.*, vol. 19, no. 12, pp. 3243–3254, Dec. 2010.

[15] K. Zhang, L. Zhang, H. Song, and D. Zhang, "Reinitialization-free level set evolution via reaction diffusion," *IEEE Trans. Image Process.*, vol. 22, no. 1, pp. 258–271, Jan. 2013.

[16] C. Samson, L. Blanc-Féraud, G. Aubert, and J. Zerubia, "A level set model for image classification," *Int. J. Comput. Vis.*, vol. 40, no. 3, pp. 187–197, 2000.

[17] N. Paragios and R. Deriche, "Coupled geodesic active regions for image segmentation: A level set approach," in *Proc. 6th Eur. Conf. Comput. Vis.*, Dublin, Ireland, Jun. 2000 , pp. 224–240.

[18] H.-K. Zhao, T. Chan, B. Merriman, and S. Osher, "A variational level set approach to multiphase motion," *J. Comput. Phys.*, vol. 127, no. 1, pp. 179–195, 1996.

[19] J. A. Bogovic, J. L. Prince, and P.-L. Bazin, "A multiple object geometric deformable model for image segmentation," *Comput. Vis. Image Understand.*, vol. 117, no. 2, pp. 145–157, 2013.

[20] L. A. Vese and T. F. Chan, "A multiphase level set framework for image segmentation using the Mumford and Shah model," *Int. J. Comput. Vis.*, vol. 50, no. 3, pp. 271–293, Dec. 2002.

[21] E. Horbert, K. Rematas, and B. Leibe, "Level-set person segmentation and tracking with multi-region appearance models and top-down shape information," in *Proc. IEEE Int. Conf. Comput. Vis. (ICCV)*, Nov. 2011, pp. 1871–1878.
[22] S. Lankton and A. Tannenbaum, "Localizing region-based active contours," *IEEE Trans. Image Process.*, vol. 17, no. 11, pp. 2029–2039, Nov. 2008.
[23] C. Li, R. Huang, Z. Ding, J. C. Gatenby, D. N. Metaxas, and J. C. Gore, "A level set method for image segmentation in the presence of intensity inhomogeneities with application to MRI," *IEEE Trans. Image Process.*, vol. 20, no. 7, pp. 2007–2016, Jul. 2011.
[24] K. Zhang, L. Zhang, K.-M. Lam, and D. Zhang, "A level set approach to image segmentation with intensity inhomogeneity," *IEEE Trans. Cybern.*, vol. 46, no. 2, pp. 546–557, Feb. 2016.
[25] X.-F. Wang, D.-S. Huang, and H. Xu, "An efficient local Chan–Vese model for image segmentation," *Pattern Recognit.*, vol. 43, no. 3, pp. 603–618, 2010.
[26] A. Gelas, O. Bernard, D. Friboulet, and R. Prost, "Compactly supported radial basis functions based collocation method for level-set evolution in image segmentation," *IEEE Trans. Image Process.*, vol. 16, no. 7, pp. 1873–1887, Jul. 2007.
[27] O. Bernard, B. Touil, A. Gelas, R. Prost, and D. Friboulet, "A RBF-based multiphase level set method for segmentation in echocardiography using the statistics of the radiofrequency signal," in *Proc. IEEE Int. Conf. Image Process. (ICIP)*, vol. 3. Sep. 2007, pp. III-157–III-160.
[28] O. Bernard, D. Friboulet, P. Thevenaz, and M. Unser, "Variational B-spline level-set method for fast image segmentation," in *Proc. 5th IEEE Int. Symp. Biomed. Imag., Nano Macro (ISBI)*, May 2008, pp. 177–180.
[29] O. Bernard and D. Friboulet, "Fast medical image segmentation through an approximation of narrow-band B-spline level-set and multiresolution," in *Proc. IEEE Int. Symp. Biomed. Imag., Nano Macro (ISBI)*, Jun. 2009, pp. 45–48.
[30] Z. Luo, M. Y. Wang, S. Wang, and P. Wei, "A level set-based parameterization method for structural shape and topology optimization," *Int. J. Numer. Methods Eng.*, vol. 76, no. 1, pp. 1–26, 2008.
[31] G. Pingen, M. Waidmann, A. Evgrafov, and K. Maute, "A parametric level-set approach for topology optimization of flow domains," *Structural Multidisciplinary Optim.*, vol. 41, no. 1, pp. 117–131, 2010.
[32] F. Mesadi, M. Cetin, and T. Tasdizen, "Disjunctive normal shape and appearance priors with applications to image segmentation," in *Medical Image Computing and Computer-Assisted Intervention MICCAI* (Lecture Notes in Computer Science), vol. 9351, N. Navab, J. Hornegger, W. Wells, and A. Frangi, Eds. Cham, Switzerland: Springer, 2015, pp. 703–710.
[33] M. U. Ghani *et al.*, "Dendritic spine shape analysis using disjunctive normal shape models," in *Proc. IEEE 13th Int. Symp. Biomed. Imag. (ISBI)*, Apr. 2016, pp. 347–350.
[34] M. U. Ghani *et al.*, "Dendritic spine classification using shape and appearance features based on two-photon microscopy," *J. Neurosci. Methods*, vol. 279, p. 13– 21, Mar. 2017.
[35] N. Ramesh, F. Mesadi, M. Cetin, and T. Tasdizen, "Disjunctive normal shape models," in *Proc. IEEE 12th Int. Symp. Biomed. Imag. (ISBI)*, Apr. 2015, pp. 1535–1539.
[36] F. Mesadi, M. Cetin, and T. Tasdizen, "Disjunctive normal level set: An efficient parametric implicit method," in *Proc. IEEE Int. Conf. Image Process. (ICIP)*, Sep. 2016, pp. 4299–4303.
[37] M. Hazewinkel, "Encyclopaedia of mathematics: C an updated and annotated translation of the soviet 'mathematical encyclopaedia'," in *Encyclopaedia of Mathematics*. The Netherlands: Springer, 1997.
[38] T. F. Chan and L. A. Vese, "Active contours without edges," *IEEE Trans. Image Process.*, vol. 10, no. 2, pp. 266–277, Feb. 2001.
[39] L. Ibanez, W. Schroeder, L. Ng, and J. Cates. *The ITK Software Guide: The Insight Segmentation and Registration Toolkit (Version1.4)*. New York, NY, USA: Kitware, 2003.
[40] L. R. Dice, "Measures of the amount of ecologic association between species," *Ecology*, vol. 26, no. 3, pp. 297–302, 1945.
[41] D. Cremers, M. Rousson, and R. Deriche, "A review of statistical approaches to level set segmentation: Integrating color, texture, motion and shape," *Int. J. Comput. Vis.*, vol. 72, no. 2, pp. 195–215, 2007.
[42] T. Dietenbeck, M. Alessandrini, D. Friboulet, and O. Bernard, "Creaseg: A free software for the evaluation of image segmentation algorithms based on level-set," in *Proc. IEEE Int. Conf. Image Process.*, Sep. 2010, pp. 665–668.
[43] N. Otsu, "A threshold selection method from gray-level histograms," *IEEE Trans. Syst., Man, Cybern.*, vol. 9, no. 1, pp. 62–66, Jan. 1979.
[44] S. M. Smith, "Fast robust automated brain extraction," *Human Brain Mapping*, vol. 17, no. 3, pp. 143–155, 2002.

Fitsum Mesadi (S'16) received the B.S. degree from Mekelle University in 2006 and the M.S. degree from the Eindhoven University of Technology in 2009, both in electrical engineering. He is currently pursuing the Ph.D. degree with the Scientific Computing and Imaging Institute, The University of Utah, UT, USA. His research interests include image analysis, computer vision, and machine learning.

Mujdat Cetin (S'98–M'02) received the Ph.D. degree in electrical engineering from Boston University, Boston, MA, USA, in 2001. From 2001 to 2005, he was with the Laboratory for Information and Decision Systems, Massachusetts Institute of Technology, Cambridge, MA, USA. Since 2005, he has been a Faculty Member with Sabanci University, Istanbul, Turkey. His research interests include statistical signal and image processing, inverse problems, radar imaging, braincomputer interfaces, machine learning, computer vision, data fusion, wireless sensor networks, biomedical information processing, and sensor array signal processing. He is currently an Area Editor for the *Journal of Advances in Information Fusion* and a Guest Editor for *Pattern Recognition Letters*.

Tolga Tasdizen (M'98–SM'09) received the B.S. degree in electrical and electronics engineering from Bogazici University, Istanbul, Turkey, in 1995, and the M.S. and Ph.D. degrees in engineering from Brown University, Providence, RI, USA, in 1997 and 2001, respectively. He held Post-Doctoral Researcher and Research Assistant Professor positions with the Scientific Computing and Imaging Institute, The University of Utah, Salt Lake City, UT, USA, from 2001 to 2004 and from 2004 to 2008, respectively. Since 2008, he has been with the Department of Electrical and Computer Engineering, The University of Utah, where he is currently an Associate Professor. He is a Faculty Member with the Utah Science Technology and Research Initiative, SCI Institute. His current research interests include image processing, computer vision, and pattern recognition with a focus on applications in biological and medical image analysis.